Emergence of Multiscale Dynamics in Colloidal Gels

Jae Hyung Cho,[1,*] Roberto Cerbino,[2] and Irmgard Bischofberger[1]
[1]Department of Mechanical Engineering, Massachusetts Institute of Technology, Cambridge, Massachusetts 02139, USA
[2]Dipartimento di Biotecnologie Mediche e Medicina Traslazionale, Università degli Studi di Milano, Via. F.lli Cervi 93, Segrate (MI) I-20090, Italy

(Received 6 November 2019; accepted 5 February 2020; published 27 February 2020)

To gain insight into the kinetics of colloidal gel evolution at low particle volume fractions ϕ, we utilize differential dynamic microscopy to investigate particle aggregation, geometric percolation, and the subsequent transition to nonergodic dynamics. We report the emergence of unexpectedly rich multiscale dynamics upon the onset of nonergodicity, which separates the wave vectors q into three different regimes. In the high-q domain, the gel exhibits ϕ-independent internal vibrations of fractal clusters. The intermediate-q domain is dominated by density fluctuations at the length scale of the clusters, as evidenced by the q independence of the relaxation time τ. In the low-q domain, the scaling of τ as q^{-3} suggests that the network appears homogeneous. The transitions between these three regimes introduce two characteristic length scales, distinct from the cluster size.

DOI: 10.1103/PhysRevLett.124.088005

Rich rheological behavior of colloidal gels arises from the coexistence of multiple length and timescales that characterize their structure and dynamics. Through particle aggregation or phase separation, colloidal gels with low particle volume fractions ϕ form space-spanning networks of self-similar clusters [1–5]. Kinetically arrested, the gels also constantly evolve towards equilibrium via structural rearrangements triggered by thermal agitation and residual stresses [6–12]. The ceaseless change in structure, in turn, leads to a continuous evolution of the dynamics. Understanding the microscopic behavior of colloidal gels, therefore, necessitates both spatially and temporally comprehensive investigation. Yet, various scattering techniques used so far to study the dynamics of gel networks have been limited by small ranges of accessible length scales and prolonged data acquisition during which the systems significantly age [13–24]. This lack of breadth in experimental characterization has prevented a coherent description of the dynamics of colloidal gels.

In this Letter, we trace the entire kinetic pathway, from stable suspensions through aged gels, of colloidal gelation and network evolution over large ranges of length and timescales using differential dynamic microscopy (DDM) [25,26]. The motion of particles and their aggregates initially slows down through two consecutive stages, while the system remains ergodic. As the gel evolves, network fluctuations become greatly suppressed, leading to the onset of nonergodicity. Three dynamically distinct ranges of length scales, or wave vectors q, then emerge, unveiling structural hierarchy and macroscopic elasticity of the gel. In the high-q domain, corresponding to length scales considerably smaller than the size of the largest aggregate units, or clusters, the network behaves as internally vibrating fractals. In the intermediate-q domain, the dynamics is dominated by the collective motion over the scale of the clusters. In the low-q domain, the gel fluctuates as a homogeneous elastic network within a viscous solvent. The transitions between these three regimes are determined by both the structure and the elasticity of the network, giving rise to two characteristic length scales. This multiscale dynamics extensively describes colloidal gels from the scale of fractal aggregates to that of a viscoelastic continuum, allowing us to estimate the macroscopic shear modulus in the latter two regimes.

This panoramic exploration of the gels throughout their evolution is enabled by DDM that, through optical microscopy, extracts information about the density fluctuations of a sample as in scattering techniques [25]. DDM is less susceptible to the effects of multiple scattering that render the use of traditional far-field scattering techniques impracticable [27]. Moreover, simultaneous access to ensemble-averaged information at several hundreds of q over more than two decades ($q = 0.05$–$10\ \mu\text{m}^{-1}$) allows the comprehensive characterization of the evolving samples. We use a CMOS camera (Prime Mono, 2048×2048 pixels, Photometrics) mounted on an inverted microscope (Eclipse TE2000-U, Nikon) with two objectives of magnifications $M = 20\times/60\times$, and numerical apertures $\text{NA} = 0.50/1.20$ (water immersion), respectively. The samples are loaded in rectangular glass capillary tubes (Vitrocom) of thickness 100 μm. We repeat some of our experiments with thicker tubes of 200 and 300 μm to check the reproducibility of the results, and confirm no influence of the finite thickness. For the computation of the normalized intermediate scattering function $f(q, \Delta t)$, where Δt denotes the delay time, we use 1000 frames acquired at frame rates from 5 fps through 100 fps.

 © 2020 American Physical Society

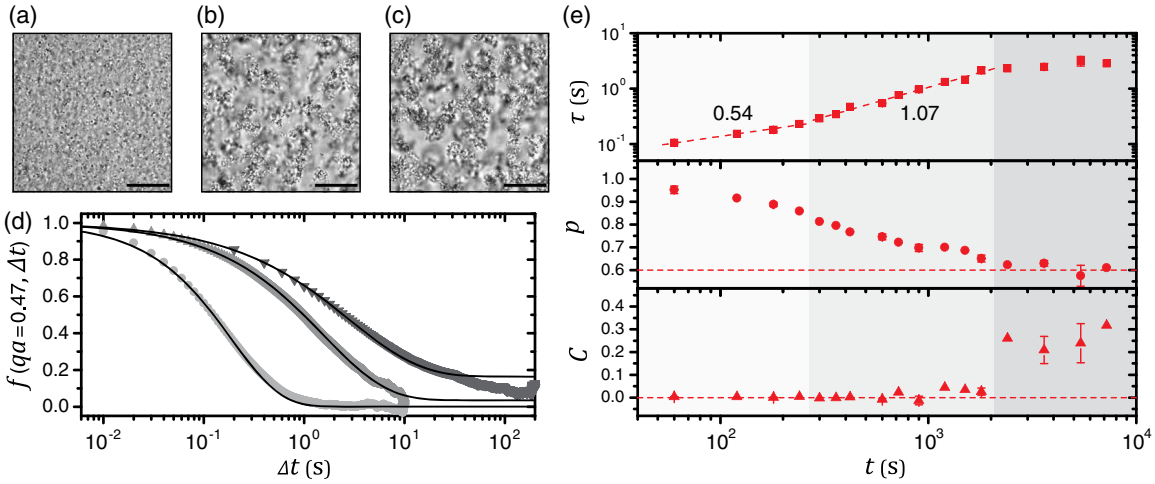

FIG. 1. Micrographs showing the temporal evolution of the gel at particle volume fraction $\phi = 0.8\%$ at times $t = 180$ s (a), 1500 s (b), and 3600 s (c) after the onset of aggregation. Scale bars correspond to 30 μm. (d) Normalized intermediate scattering function f at $t = 180$ s (circle), 1500 s (triangle), 3600 s (inverted triangle), and corresponding fits (black lines) at a fixed wave vector $q = 4.0\ \mu\text{m}^{-1}$ or $qa = 0.47$, where $a = 116.3$ nm is the hydrodynamic radius of a particle. (e) Temporal evolution of the relaxation time τ, the stretching exponent p, and the nonergodicity parameter C at $qa = 0.47$. Some error bars are smaller than the symbols.

We utilize polystyrene-poly(N-isopropylacrylamide) (PS-PNIPAM) core-shell colloidal particles synthesized by emulsion polymerization based on the protocol of Refs. [22,28]. The details of the synthesis are described in the Supplemental Material [29]. Because of the thin, thermosensitive PNIPAM shell, we can precisely control the initiation of the gelation from a fully stable suspension simply by increasing the system temperature T above the gelation temperature $T_g \approx 25.5\,^{\circ}\text{C}$. The increase in T reduces the range of the steric repulsion from the shell, allowing the particles to aggregate by van der Waals attraction. To minimize the effect of electrostatic interactions and sedimentation, we add 0.5 M of sodium thiocyanate (NaSCN) to screen the charges, and density-match the system using a H_2O/D_2O mixture of 52/48 v/v. The hydrodynamic radius a of the particles measured via dynamic light scattering (BI-200SM, Brookhaven Instruments) is 116.3 ± 1.8 nm at 30 °C.

We initiate the gelation of a system at $\phi = 0.8\%$ by a sudden temperature increase from 20 to 30 °C at $t = 0$ s. To quantify the dynamics at different t in the micrographs as the ones shown in Figs. 1(a)–1(c), we focus on the fast dynamics of colloidal gels due to thermal fluctuations [14], by assuming the following form of $f(q, \Delta t)$

$$f(q, \Delta t) = [1 - C(q)] \exp\left[-\left(\frac{\Delta t}{\tau(q)}\right)^{p(q)}\right] + C(q), \qquad (1)$$

which represents a stretched exponential decay from one to the nonergodicity parameter $C(q)$. Here, $\tau(q)$ denotes the relaxation time, and $p(q)$ the stretching exponent. Because of the subsequent relaxation due to slow restructuring of the network [9], the large Δt behavior of $f(q, \Delta t)$ often deviates from the fit, as displayed in Fig. 1(d), but this long-time behavior is outside the scope of this work. The details of the fitting procedures are delineated in the Supplemental Material [29].

In the first stage until $t \approx 250$ s, the particles form aggregates, as seen in Fig. 1(a). The temporal change of the relaxation time $\tau(q)$ at $q = 4.0\ \mu\text{m}^{-1}$ or $qa = 0.47$, shown in Fig. 1(e), exhibits a power law with an exponent 0.54 ± 0.05; this growth rate is similar to that of diffusion-limited cluster aggregation (DLCA) [1,2]. In DLCA, the mean hydrodynamic radius R_h of aggregates scales as $t^{1/d_f} = t^{0.57}$ with the fractal dimension $d_f = 1.75$ [2,32,33]. Using $\tau = 1/(Dq^2)$, where D is the diffusion coefficient of the aggregates, and the Stokes-Einstein relation $D = k_B T/(6\pi\eta R_h)$, where k_B is the Boltzmann constant and η the solvent viscosity [34], we can indeed infer that $\tau(t)$ obeys the same power law as $R_h(t)$. Moreover, from the static structure factor $S(q)$ that we calculate based on the squared modulus of Fourier-transformed images [27,35], we find that d_f of the aggregates is 1.8 ± 0.1 [4,29], independent of t, also in close agreement with DLCA. Although the two relations involving D strictly apply to suspensions of monodisperse particles, the power law exponent of $\tau(t)$ stays nearly independent of q, confirming the resemblance of the aggregation to DLCA.

The second stage of evolution (250 s $< t <$ 2000 s) in Fig. 1(e) displays a steeper power law of $\tau(t)$ with an exponent 1.07 ± 0.04, while $p(t)$ monotonically decreases to ~0.6. We suggest that this transition to the second stage is induced by the geometric percolation of the clusters. As the percolation starts to constrain the displacements of the clusters, a marked slowdown of their motion ensues, inducing greater heterogeneity in relaxation times. The stretched exponential relaxation of colloidal gels is generally understood as the superposition of the multiple

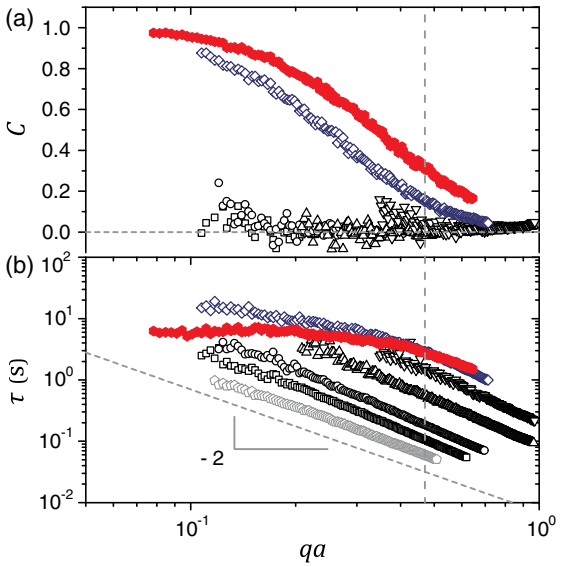

FIG. 2. (a) Nonergodicity parameter C and (b) relaxation time τ of the gel at $\phi = 0.8\%$ as a function of the nondimensionalized wave vector qa at $t = 0$ s (pentagon, stable suspension), 60 s (square), 180 s (circle), 600 s (triangle), 1500 s (inverted triangle), 3600 s (diamond), and 7200 s (filled hexagon). The dashed vertical line denotes $qa = 0.47$ corresponding to the data in Fig. 1.

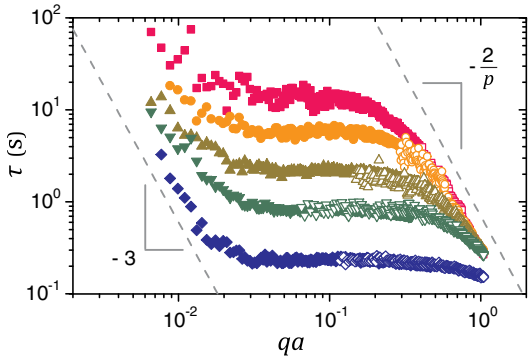

FIG. 3. Relaxation time τ of the aged gels in quasisteady states as a function of the nondimensionalized wave vector qa at $\phi = 0.5\%$ (square), 0.8% (circle), 1.0% (triangle), 1.5% (inverted triangle), and 2.0% (diamond). Filled symbols denote data obtained with a 20× objective and open symbols with a 60× objective.

normal modes subject to overdamped dynamics, each exhibiting a single exponential decay [14]. In this framework, the distribution of characteristic timescales of the exponentials broadens as p decreases from 1 to approximately 0.65 [36]. At all t, p is largely independent of q [29]. Despite these temporal changes in τ and p, the system retains its ergodicity, which implies that the structural rearrangements after the geometric percolation only gradually give rise to rigidity of the network [37,38].

After the onset of the third stage ($t \approx 2000$ s) shown in Fig. 1(e), the network fluctuations remain partially correlated within the observation time, leading to nonzero values of the nonergodicity parameter $C(q = 4.0\ \mu\text{m}^{-1})$. Concurrently, $\tau(q = 4.0\ \mu\text{m}^{-1})$ stays nearly constant with t. Yet, complex q dependence of the dynamics appears upon this transition. For $t < 2000$ s, $C(q) \approx 0$ while $\tau(q) \sim q^{-2.2}$, where the power law exponent is close to -2 of the dilute suspension of monodisperse particles in Brownian motion [34]. For $t > 2000$ s, however, $C(q)$ gradually increases with t while monotonically decreasing with q, as displayed in Fig. 2(a). Simultaneously, $\tau(q)$ flattens, and eventually becomes independent of q for $qa < 0.23$, as shown in Fig. 2(b). This flattening of $\tau(q)$ marks the end of major temporal evolution, after which all the parameters remain nearly unchanged.

For a more comprehensive inspection of the q dependence of the dynamics in the aged gels, we employ two objectives ($M = 20\times$ and $60\times$) to extract $\tau(q)$ of the gels at five different ϕ (= 0.5, 0.8, 1.0, 1.5, and 2.0%) in their quasisteady states at sufficiently large t. For each ϕ, three distinct regimes of dynamics emerge, as displayed in Fig. 3. In the remainder of this Letter, we show how this transition into nonergodic, multiscale dynamics reveals the structure and the macroscopic elasticity of the gels.

In the high-q domain, we observe dynamical hallmarks of fractals. The averaged internal structure of fractal aggregates is fully defined by d_f only, and indeed, $\tau(q)$ of all ϕ asymptotically collapse onto a single line, indicating the presence of ϕ-independent structures at the smallest length scales probed. Furthermore, according to the model proposed by Reuveni *et al.* [39,40], the internal dynamics of a vibrating fractal under thermal perturbation and strong viscous damping for $qR_g \gg 1$, where R_g is the cluster radius of gyration, obeys the following scaling relation in the absence of translation and rotation:

$$\tau \sim q^{-2/p}. \tag{2}$$

We obtain $p = 0.66 \pm 0.02$ for all ϕ [29], which yields the value of $-2/p$ consistent with our high-q power law exponent.

In the intermediate-q domain, where τ is independent of q, the motion at the length scale of clusters dominates the gel dynamics. In the model developed by Krall and Weitz for fractal gels [13,14], $f(q, \Delta t)$ is determined by τ and the maximum mean squared displacement δ^2 at the length scale of the clusters as follows:

$$f(q, \Delta t) = \exp\left(-\frac{q^2\delta^2}{4}\left\{1 - \exp\left[-\left(\frac{\Delta t}{\tau}\right)^p\right]\right\}\right), \tag{3}$$

which, for $q^2\delta^2 \ll 1$, can be simplified to

$$f(q, \Delta t) \approx \frac{q^2\delta^2}{4}\exp\left[-\left(\frac{\Delta t}{\tau}\right)^p\right] + \left(1 - \frac{q^2\delta^2}{4}\right), \tag{4}$$

an equivalent functional form to our model in Eq. (1). From Eqs. (1) and (3) in the limit of $\Delta t \to \infty$,

$$f(q, \Delta t \to \infty) = \exp\left(-\frac{q^2\delta^2}{4}\right) = C(q). \tag{5}$$

The resulting δ^2 from curve fits to $C(q)$ satisfies $q^2\delta^2 \ll 1$ for the intermediate-q domain [29]. Provided that the microscopic elasticity of the gels is governed by the local spring constant $\kappa \sim (a/\xi)^\beta$ between two particles of radius a separated by the distance ξ within a fractal cluster, where β is the elasticity exponent [41–43], τ and δ^2 scale with ϕ as

$$\tau \sim \phi^{-(\beta+1)/(3-d_f)}, \qquad \delta^2 \sim \phi^{-\beta/(3-d_f)}, \tag{6}$$

respectively [14]. We measure the mean value of the q-independent relaxation time τ_m, and observe the scalings of $\tau_m \sim \phi^{-2.93\pm0.15}$ and $\delta^2 \sim \phi^{-2.07\pm0.04}$. With $d_f = 1.8$, consistent values of $\beta = 2.52 \pm 0.18$ and 2.48 ± 0.05, respectively, are obtained, which reflect considerable structural rearrangements during the network formation [29,42,44,45].

We demonstrate that our model simultaneously exhibits the dynamics described in the two models by Reuveni *et al.* [40] and by Krall and Weitz [14], as it separates the q dependence of the characteristic relaxation time and that of the nonergodicity into two parameters $\tau(q)$ and $C(q)$, respectively, in Eq. (1). The anomalous diffusion of the subcluster aggregates is ergodic for $qR_g \gg 1$ [40], while the fluctuations at the length scale of the clusters are nonergodic [14]. Yet, the q^2 term in Eq. (3) determines the q dependence of both the timescale of the decay and the plateau of f as $\Delta t \to \infty$, by assuming nonergodic processes at all q [14,29]. In our model, $\tau(q)$ and $C(q)$ allow independent determination of within what time and how far, respectively, scatterers move at each q. We thus suggest that, at the transition between the intermediate-q and the high-q regimes, the relaxation time of the internal vibrations captured in Eq. (1) simply scales as τ_m, which from Eqs. (2) and (6) leads to

$$q_h \sim \phi^{[p(\beta+1)]/[2(3-d_f)]}, \tag{7}$$

where q_h denotes the intermediate-to-high-q transition wave vector. With $p = 0.66$ and $\beta = 2.50$, Eq. (7) yields $q_h \sim \phi^{0.96\pm0.07}$. Using q_h and τ_m to scale q and $\tau(q)$, we find that our data of all ϕ collapse onto a master curve in the plateau and the high-q domain, as shown in Fig. 4(a).

In the low-q regime, the gels display overdamped dynamics characteristic of a homogeneous viscoelastic medium. The effective spring constant κ between two particles is independent of their distance ξ, if ξ is greater than the smallest length scale L at which the continuum assumption holds true [46]. The magnitude of the frictional force that a scatterer experiences in a homogeneous

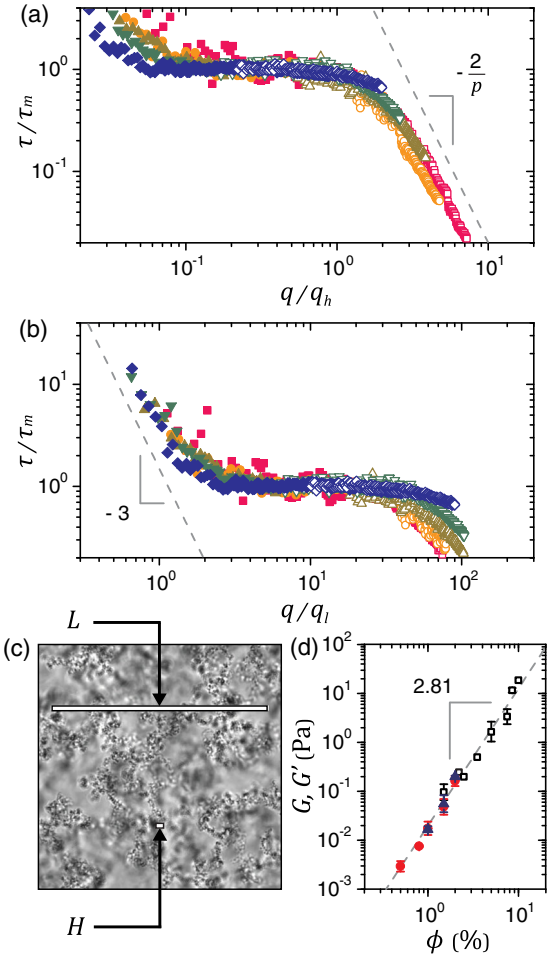

FIG. 4. Relaxation time τ of all ϕ scaled with the wave vectors at the intermediate-to-high-q transition q_h (a) or the low-to-intermediate-q transition q_l (b) in the abscissa and the mean τ of the intermediate-q domain τ_m in the ordinate. (c) Micrograph of the aged gel at $\phi = 0.8\%$. Scale bars indicate the transition length scales $H = 2\pi/q_h \approx 3.3$ μm, and $L = 2\pi/q_l \approx 99.4$ μm. (d) Storage modulus G' (square) obtained from conventional rheometry and shear modulus G estimated from DDM in the intermediate-q (filled circle) and the low-q (filled triangle) domains. The DDM estimates show consistent power laws.

two-phase continuum, however, scales as its volume V [47,48], as every differential volume undergoes the same amount of viscous coupling between the two phases. Because of the tenuous and porous structure of the network, the total frictional force is expected to be proportional to the number of constituent particles N, which in a continuum scales as $N \sim \phi V$. Thus, in the low-q domain,

$$\tau \sim \frac{\eta a(\phi V/a^3)}{GL} \sim \frac{\eta\phi q_l}{Ga^2} q^{-3}, \tag{8}$$

where $G \sim \kappa/L$ denotes the macroscopic shear modulus, with L chosen as the characteristic length scale of the elastic forces and $q_l = 2\pi/L$. Indeed, $\tau(q)$ at $\phi = 2.0\%$

exhibits the scaling of $\tau \sim q^{-3}$ for $qa < 0.012$, as shown in Fig. 3. For Eq. (8) to be valid at all ϕ, we expect $\tau(q) = \psi(\phi)q^{-3}$, where $\psi(\phi) \sim \tau_m(\phi)q_l(\phi)^3$. Because τ_m denotes the timescale of the floppiest mode of the gel network, it also sets G by

$$G = \frac{6\pi\eta b_m}{\tau_m}, \tag{9}$$

where b_m is a correction factor [14]. Substituting the general form of $\tau(q)$ into Eq. (8) and using $\tau_m(\phi) \sim G(\phi)^{-1}$ from Eq. (9), therefore, results in

$$q_l \sim \phi^{0.5}. \tag{10}$$

Scaling $\tau(q)$ of all ϕ with the resulting q_l leads to a master curve in the low-q and the intermediate-q domains, as shown in Fig. 4(b). The power law in Eq. (10) differs from that of the DLCA cluster radius ${R_c}^{-1} \sim \phi^{1/(3-d_f)} = \phi^{0.8}$ [41], since the macroscopic elasticity, as well as the structure, governs the dynamical length scale L. We insert scale bars of length $L = 2\pi/q_l$ and $H = 2\pi/q_h$ in Fig. 4(c) at $\phi = 0.8\%$, to visually highlight the contrast between the length scales of the low-q and the high-q regimes.

The direct link between τ and G indicates that we can estimate the macroscopic shear modulus G of the gels by measuring the microscopic relaxation time τ in either the intermediate-q domain or, as long as we can identify q_l, the low-q domain. Using Eq. (9) with $b_m = 2.8$, we observe that the resulting values of G yield a smooth continuation of the storage modulus G' obtained from conventional rheometry (AR-G2, TA Instruments), as shown in Fig. 4(d). Alternatively, G can be estimated by measuring ψ and q_l from Fig. 3, if the power law behavior of $\tau \sim q^{-3}$ is accessible. The following rearranged form of Eq. (8)

$$G = \frac{\eta\phi q_l b_l}{a^2\psi}, \tag{11}$$

where $b_l = 1.2$ is a correction factor, yields consistent scaling behavior of G, as displayed in Fig. 4(d).

Our dynamical investigation of evolving colloidal gels unveils the extensive kinetic route through particle aggregation, geometric percolation, and the emergence of nonergodicity that establishes distinct dynamical regimes at different length scales. In particular, we show that internal vibrations of random fractals, cluster-dominated fluctuations, and the homogeneity of a viscoelastic medium simultaneously define the nonergodic colloidal gels. Consequently, our results not only demonstrate links among different models, but clarify their limits. We expect similar applications of DDM to other types of soft matter, such as biopolymer particle-network mixtures [49,50] or dense suspensions of active particles [51,52], can likewise provide comprehensive descriptions of their nonergodic, multiscale dynamics [53].

We thank Veronique Trappe and Fabio Giavazzi for helpful discussions. J. H. C. and I. B. acknowledge support from the MIT Research Support Committee and Kwanjeong Educational Foundation, Awards No. 16AmB02M and No. 18AmB59D. R. C. acknowledges support from Regione Lombardia and CARIPLO Foundation, Grant No. 2016-0998.

*Corresponding author.
jaehcho@mit.edu

[1] P. Meakin, Phys. Rev. Lett. **51**, 1119 (1983).
[2] D. A. Weitz and M. Oliveria, Phys. Rev. Lett. **52**, 1433 (1984).
[3] M. Y. Lin, H. M. Lindsay, D. A. Weitz, R. C. Ball, R. Klein, and P. Meakin, Phys. Rev. A **41**, 2005 (1990).
[4] M. Carpineti and M. Giglio, Phys. Rev. Lett. **68**, 3327 (1992).
[5] P. J. Lu, E. Zaccarelli, F. Ciulla, A. B. Schofield, F. Sciortino, and D. A. Weitz, Nature (London) **453**, 499 (2008).
[6] E. Zaccarelli, J. Phys. Condens. Matter **19**, 323101 (2007).
[7] R. N. Zia, B. J. Landrum, and W. B. Russel, J. Rheol. **58**, 1121 (2014).
[8] Y. Gao, J. Kim, and M. E. Helgeson, Soft Matter **11**, 6360 (2015).
[9] L. Cipelletti, S. Manley, R. C. Ball, and D. A. Weitz, Phys. Rev. Lett. **84**, 2275 (2000).
[10] S. Manley, B. Davidovitch, N. R. Davies, L. Cipelletti, A. E. Bailey, R. J. Christianson, U. Gasser, V. Prasad, P. N. Segrè, and M. P. Doherty *et al.*, Phys. Rev. Lett. **95**, 048302 (2005).
[11] J. M. van Doorn, J. Bronkhorst, R. Higler, T. van de Laar, and J. Sprakel, Phys. Rev. Lett. **118**, 188001 (2017).
[12] M. Bouzid, J. Colombo, L. V. Barbosa, and E. Del Gado, Nat. Commun. **8**, 15846 (2017).
[13] A. H. Krall, Z. Huang, and D. A. Weitz, Physica (Amsterdam) **235A**, 19 (1997).
[14] A. H. Krall and D. A. Weitz, Phys. Rev. Lett. **80**, 778 (1998).
[15] P. N. Segrè, V. Prasad, A. B. Schofield, and D. A. Weitz, Phys. Rev. Lett. **86**, 6042 (2001).
[16] S. Manley, H. M. Wyss, K. Miyazaki, J. C. Conrad, V. Trappe, L. J. Kaufman, D. R. Reichman, and D. A. Weitz, Phys. Rev. Lett. **95**, 238302 (2005).
[17] M. Laurati, G. Petekidis, N. Koumakis, F. Cardinaux, A. B. Schofield, J. M. Brader, M. Fuchs, and S. U. Egelhaaf, J. Chem. Phys. **130**, 134907 (2009).
[18] S. Romer, F. Scheffold, and P. Schurtenberger, Phys. Rev. Lett. **85**, 4980 (2000).
[19] F. Scheffold, S. E. Skipetrov, S. Romer, and P. Schurtenberger, Phys. Rev. E **63**, 061404 (2001).
[20] H. M. Wyss, S. Romer, F. Scheffold, P. Schurtenberger, and L. J. Gauckler, J. Colloid Interface Sci. **241**, 89 (2001).
[21] J. Liu, V. Boyko, Z. Yi, and Y. Men, Langmuir **29**, 14044 (2013).
[22] D. C. E. Calzolari, I. Bischofberger, F. Nazzani, and V. Trappe, J. Rheol. **61**, 817 (2017).
[23] H. Guo, S. Ramakrishnan, J. L. Harden, and R. L. Leheny, J. Chem. Phys. **135**, 154903 (2011).

[24] Q. Zhang, D. Bahadur, E. M. Dufresne, P. Grybos, P. Kmon, R. L. Leheny, P. Maj, S. Narayanan, R. Szczygiel, S. Ramakrishnan, and A. Sandy, Phys. Rev. Lett. **119**, 178006 (2017).
[25] R. Cerbino and V. Trappe, Phys. Rev. Lett. **100**, 188102 (2008).
[26] F. Giavazzi, D. Brogioli, V. Trappe, T. Bellini, and R. Cerbino, Phys. Rev. E **80**, 031403 (2009).
[27] F. Giavazzi and R. Cerbino, J. Opt. **16**, 083001 (2014).
[28] N. Dingenouts, C. Norhausen, and M. Ballauff, Macromolecules **31**, 8912 (1998).
[29] See the Supplemental Material at http://link.aps.org/supplemental/10.1103/PhysRevLett.124.088005 for the synthesis protocol and the characterization of the PS-PNIPAM particles, the curve-fitting method, and more details of our DDM analysis, which includes Refs. [30,31].
[30] F. Giavazzi, P. Edera, P. J. Lu, and R. Cerbino, Eur. Phys. J. E **40**, 97 (2017).
[31] P. Meakin, I. Majid, S. Havlin, and H. E. Stanley, J. Phys. A **17**, L975 (1984).
[32] D. A. Weitz, J. S. Huang, M. Y. Lin, and J. Sung, Phys. Rev. Lett. **53**, 1657 (1984).
[33] P. G. J. van Dongen and M. H. Ernst, Phys. Rev. Lett. **54**, 1396 (1985).
[34] P. N. Pusey, in *Neutrons, X-rays and Light: Scattering Methods Applied to Soft Condensed Matter*, edited by P. Lindner and T. Zemb (Elsevier, Amsterdam, 2002), 1st ed., Chap. 9.
[35] P. J. Lu, F. Giavazzi, T. E. Angelini, E. Zaccarelli, F. Jargstorff, A. B. Schofield, J. N. Wilking, M. B. Romanowsky, D. A. Weitz, and R. Cerbino, Phys. Rev. Lett. **108**, 218103 (2012).
[36] D. C. Johnston, Phys. Rev. B **74**, 184430 (2006).
[37] H. Tsurusawa, M. Leocmach, J. Russo, and H. Tanaka, Sci. Adv. **5**, eaav6090 (2019).
[38] S. Zhang, L. Zhang, M. Bouzid, D. Z. Rocklin, E. Del Gado, and X. Mao, Phys. Rev. Lett. **123**, 058001 (2019).
[39] S. Reuveni, J. Klafter, and R. Granek, Phys. Rev. Lett. **108**, 068101 (2012).
[40] S. Reuveni, J. Klafter, and R. Granek, Phys. Rev. E **85**, 011906 (2012).
[41] W. H. Shih, W. Y. Shih, S. I. Kim, J. Liu, and I. A. Aksay, Phys. Rev. A **42**, 4772 (1990).
[42] R. de Rooij, D. van den Ende, M. H. G. Duits, and J. Mellema, Phys. Rev. E **49**, 3038 (1994).
[43] A. H. L. West, J. R. Melrose, and R. C. Ball, Phys. Rev. E **49**, 4237 (1994).
[44] Y. Kantor and I. Webman, Phys. Rev. Lett. **52**, 1891 (1984).
[45] S. Romer, H. Bissig, P. Schurtenberger, and F. Scheffold, Europhys. Lett. **108**, 48006 (2014).
[46] A. D. Dinsmore, V. Prasad, I. Y. Wong, and D. A. Weitz, Phys. Rev. Lett. **96**, 185502 (2006).
[47] A. J. Levine and T. C. Lubensky, Phys. Rev. Lett. **85**, 1774 (2000).
[48] A. J. Levine and T. C. Lubensky, Phys. Rev. E **63**, 041510 (2001).
[49] D. M. Wulstein, K. E. Regan, J. Garamella, R. J. McGorty, and R. M. Robertson-Anderson, Sci. Adv. **5**, eaay5912 (2019).
[50] F. Burla, T. Sentjabrskaja, G. Pletikapic, J. van Beugen, and G. H. Koenderink, Soft Matter **16**, 1366 (2020).
[51] L. M. C. Janssen, J. Phys. Condens. Matter **31**, 503002 (2019).
[52] L. Berthier, E. Flenner, and G. Szamel, J. Chem. Phys. **150**, 200901 (2019).
[53] R. Cerbino and P. Cicuta, J. Chem. Phys. **147**, 110901 (2017).